ELSEVIER

International Journal of Heat and Fluid Flow 23 (2002) 564–571

International Journal of HEAT AND FLUID FLOW

www.elsevier.com/locate/ijhff

Wake flow in adverse pressure gradient

David M. Driver [a,*], George G. Mateer [b]

[a] NASA Ames Research Center M/S 260-1, Moffett Field, CA 94035, USA
[b] MCAT Institute, Los Gatos, CA 95030, USA

Abstract

In the interest of improving the predictability of high-lift systems at maximum lift conditions, a series of fundamental experiments were conducted to study the effects of adverse pressure gradient on a wake flow. Mean and fluctuating velocities were measured with a two-component laser-Doppler velocimeter. Data were obtained for several cases of adverse pressure gradient, producing flows ranging from no reversed flow to massively reversed flow. While the turbulent Reynolds stresses increase with increasing size of the reversed flow region, the gradient of Reynolds stress $(-\partial\overline{uv}/\partial y)$ does not. Computations using various turbulence models were unable to reproduce the reversed flow.

1. Introduction

The maximum lift developed by multi-element airfoils can be limited by flow reversals in the wake of the main element as seen by Brune and Sikavi (1983), Rogers (1993) and Chin et al. (1993). The off-body separation can lead to de-cambering of the multi-element airfoil system and an associated loss of lift. Turbulent mixing in the wake controls the growth of the wake and dictates the extent to which the wake experiences flow reversal. Consequently, subtle differences in turbulence models make a significant difference in the prediction of wake growth. Failure to accurately predict the wake spreading rate can lead to inaccuracies in the prediction of maximum lift.

In an effort to understand the spreading rate of wakes in adverse pressure gradient, there have been several experiments in simplified geometrical flow fields by Hoffenberg and Sullivan (1998), Hoffenberg et al. (1995), Roos (1997), Xiaofeng et al. (1999), Pot (1979), Adaire and Horne (1988) and Tummers et al. (1997). These wake flow experiments have been conducted on a variety of zero and "mildly" adverse pressure gradient flows. This paper presents experimental results on a wake flow with flow reversals using a simplified geometry in which an adverse pressure gradient (streamline divergence) is developed without the complication of lift, curvature and transition effects. Symmetry of the test section and flow field make it easier to analyze and understand "off-body" separation (as it is often called). Later in the study, curvature and Reynolds number effects were added without significantly complicating the flow field. The variable known as "overhang" to the high lift community was also studied by virtue of varying the length of the trailing edge into the pressure gradient. This is part of an overall effort to improve predictions of maximum lift for multi-element airfoils. The data are intended for use in guiding turbulence modeling for such flows.

2. Experiment

Experiments were performed in the High Reynolds Channel Number 1, a pressurized wind tunnel at NASA Ames Research Center. The test section (Fig. 1) consisted of a straight section of duct, 108 mm tall × 381 mm wide duct (450 mm long), followed by a variable angle 2D divergent section which exhausted into an adjacent straight section. A flat plate 6 mm thick, 381 mm wide and 419 mm long was mounted in the center of the straight section of duct and fixed parallel to the wind tunnel walls so as to equally split the flow in the top and bottom halves of the 108 mm tall channel. The downstream 38-mm of the plate was symmetrically and linearly tapered to a 0.4 mm trailing edge. The upstream edge was a circular arc.

* Corresponding author.
E-mail addresses: ddriver@mail.arc.nasa.gov (D.M. Driver), gmateer@worldnet.att.net (G.G. Mateer).

0142-727X/02/$ - see front matter
PII: S0142-727X(02)00152-2

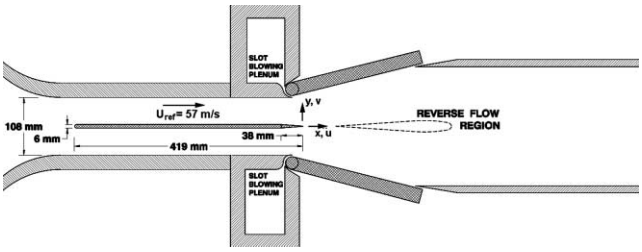

Fig. 1. Test section geometry.

The test section is uniform in the span-wise direction and the developing flow is nominally two-dimensional. The tunnel wall boundary layers were prevented from separating with jets issuing tangentially from slots on all four walls of the tunnel. Flow in the duct was held at a constant Mach number of 0.175 by virtue of a choked convergent nozzle downstream. The tunnel was pressurized to 5.5 atmospheres which produced a Reynolds number based on plate length of 10 million. Velocity surveys performed in the straight section of duct, well ahead of the divergent section, indicate that the boundary layer on the splitter plate (350 mm downstream of plate leading edge) is turbulent and approximately 5 mm thick. Here the momentum thickness was determined to be 0.55 mm. These measurements serve as initial conditions (or conditions that were matched) for CFD calculations.

Data were obtained with a two-component LDV system with a 100 μm interrogation volume operating in back scatter and using Fourier transform signal processing. Uncertainties are estimated to be ±1% on velocity and ±15% on the Reynolds shear stress ($-\overline{uv}$). normal Reynolds stress components ($\overline{u^2}$ and $\overline{v^2}$) were also measured, but are not reported here. Pressures and skin friction were also measured on the wind tunnel surfaces with uncertainties of ±0.02 for C_p and ±10% for C_f.

Two dimensionality of each flow field was checked with: (1) oil flow visualization of the trailing edge, (2) spanwise measurements of pressure at the trailing edge, (3) spanwise measurements of velocity at the location $x = 190$ mm (where the velocity deficit is greatest), (4) and mass and momentum balance on the channel. In each case two-dimensionality was found to be excellent over the central 2/3 of the test section, with the exception of the massively separated test case.

Boundary layer control was accomplished with 0.2 mm wide jets (directed tangentially) built into the divergent wall hinges and 0.5 mm jets on the side walls. The jet velocities were nearly sonic at the exit and the mass flow of all four jets combined was approximately 2% of the total tunnel mass flow. The jet mass flow rate was adjusted to the minimum amount necessary to achieve attached flow on all four walls as determined from oil flow visualizations. The side wall jets were sufficiently energetic to prevent separation on the side walls as seen in oil flow visualization and LDV measurements.

3. Computations

Computations were performed on each of the experimental test cases using the INS2D code of Rogers and Kwak (1990, 1991). This code solves the incompressible Navier–Stokes equations in two-dimensional generalized coordinates for both steady-state and time varying flow using a pseudo-compressibility method. The convective terms are differenced using an upwind biased flux-difference splitting. The equations are solved using an implicit line-relaxation scheme. The turbulence models of Spalart and Allmaras (1994) (SA) and Menter (1993) (SST) were used in the computations. Symmetric flows were calculated over the upper half of the channel only using a 120×81 grid shown in Fig. 2. Note that the figure is expanded in the vertical direction. It should be noted that the Menter (1993) SST model is a blend of k–ω near surfaces and k–ε away from surfaces,

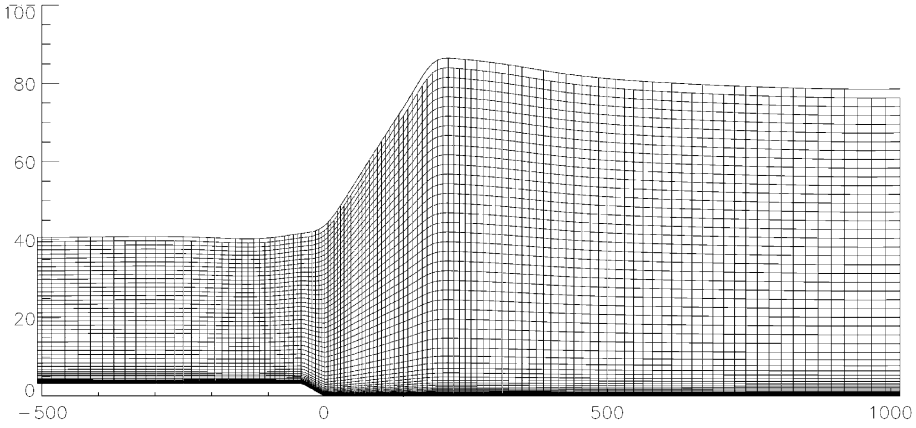

Fig. 2. Grid of 120×81 used in INS2D solutions.

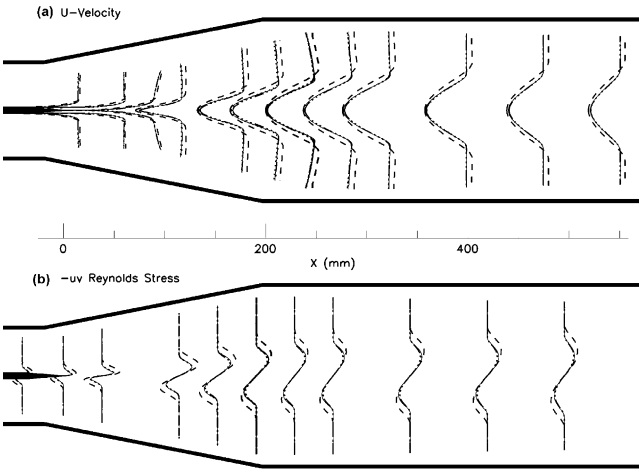

Fig. 3. Computed velocity and $-\overline{uv}$ Reynolds stress profiles performed on grids of 60×41 (– – –), 90×54 (— · ·), 120×81 (· · · · ·), and 240×162 (—).

consequently, in the region of interest (the wake) the model is essentially a k–ε turbulence model.

In the computations, the length of inlet duct was adjusted so that the boundary layer momentum thickness in the computation matched that of the experiment ($\theta = 0.55$ mm at $x = -88.9$ mm). The upper boundary in the computation was obtained by imposing a "slip" condition on a measured streamline. A streamline was chosen which was far enough from the tunnel wall so as to be outside the wall jet and also outside the viscous region of the wake. A "no slip" condition was imposed on the splitter plate and symmetry conditions were imposed on the centerline of the wake. To verify that the symmetry boundary condition was working properly, a calculation was performed on the full channel (240×81 grid) and compared to a calculation of the upper half channel only (120×81 grid), showing no differences.

A grid resolution study was performed on the strongly adverse pressure gradient test case shown in Fig. 2. Grids of 60×41, 90×54, 120×81, and 240×162 were used in computations of this test case, employing the SA turbulence model. Velocity profiles and $-\overline{uv}$ Reynolds stress profiles are shown at a series of stream-wise locations (Fig. 3). The computations using the 90×54, 120×81, and 240×162 grids are virtually identical. Only the computation using the 60×41 grid differs from the other three computations. Subsequent calculations presented in this paper were performed on grids of 120×81 (for symmetric cases).

4. Results

Several configurations were tested in which the wake was passed through a variety of symmetric diffusers as well as an asymmetric diffuser. Flow fields ranged from

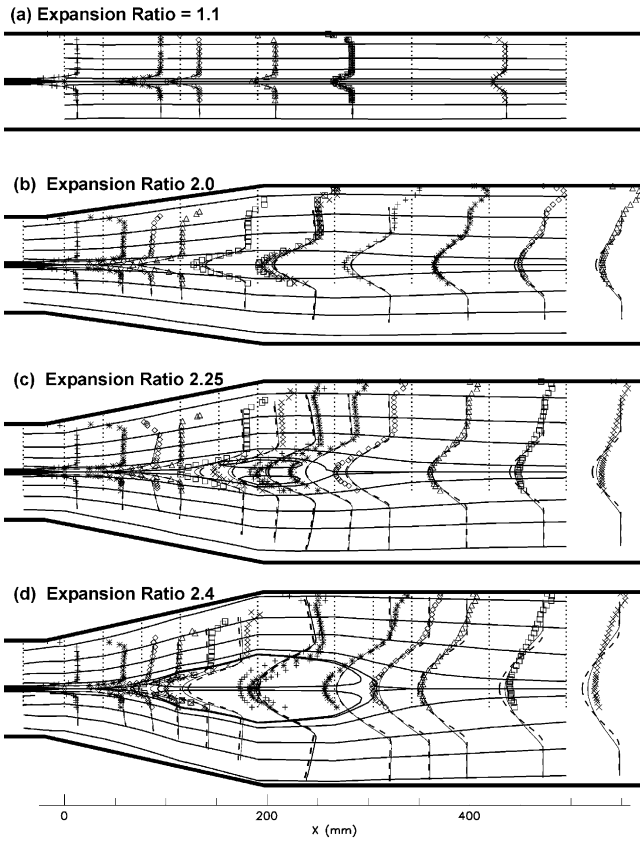

Fig. 4. Measured and computed velocity profiles for various tunnel geometries, streamlines overlaid. SST (—), SA (– – –) models, experiment (symbols).

strong adverse pressure gradient without reversed flow, to flows with small and massive reversed flow regions (Fig. 4). A straight wall case was also measured in order to provide a baseline for the divergent cases (Fig. 4). Each case has been heavily documented with LDV measurements.

The streamlines shown in Fig. 4 were determined experimentally by evaluating stream functions using the velocity measurements. The geometric centerline was assumed to be the zero stream function. Velocity measurements were obtained only in the upper 60% of the channel due to optical access limitations. Velocities in the lower third of the channel were assumed to be the same as the upper third of the channel for the purpose of computing stream function. To the extent that data exists below the symmetry plane, good symmetry can be seen. Velocity profiles at several span-wise stations ($z = 0$, $z = +0.23w$, and $z = -0.23w$) are shown for the $x = 190$ mm location, indicating good two-dimensionality of the flow where z is the distance from the tunnel centerline and w is the width of the tunnel. Good mass conservation is evident by virtue of the outer most streamline conforming to the tunnel wall. The massively separated case (expansion ratio = 2.4) is the excep-

tion—here the effects of three-dimensionality are probably causing the deviation of the outer streamline with respect to the tunnel wall. While the massively separated case is probably not a good test case for CFD validation, it is useful for understanding turbulent transport and will be discussed in that vein.

The tangential jet blowing along the upper wall of the wind tunnel can be seen in the velocity profiles. No jet blowing is used in the straight wall test case.

Computations using either the SST or SA turbulence models have no difficulty predicting the straight wall test case. However, in the strong adverse pressure gradient cases the computations produce less velocity deficit than that seen in the experiment. No reversed flow is seen in the small separation case (expansion ratio = 2.25) and only a minimal region of reversed flow is produced by the SST model in the case with massive separation (expansion ratio = 2.4).

It should be noted that the expansion ratio quoted for each test case is derived from the area under the measured stream function. A non-zero expansion ratio for the straight wall test case is attributable to the splitter plate thickness variation and boundary layer growth on the test section walls. The expansion ratio derived from streamlines is very nearly the same as that derived from tunnel geometry. Table 1 gives the outer streamline position for each of the test cases described in this paper—these streamlines were used in the computations. The numbers in italics in the table were not measured, they were extrapolated values used to extend the computational domain. Also no data was obtained where a dash appears in the table.

Reynolds shear stress ($-\overline{uv}$) was also measured for each test case (see Fig. 5). For the straight wall case (expansion ratio = 1.1) the Reynolds shear stress decays rapidly with distance from the splitter plate trailing edge. Both calculations agree well with the data for this case. As the channel divergence increases so does the shear stress. Both calculations under-predict the magnitude of the shear stress for the strong adverse pressure gradient cases. Good spanwise uniformity is seen again at the $x = 190$ mm station where profiles at stations $z = 0$, $z = +0.23w$, and $z = -0.23w$ can be seen. The exception once again being the massively separated case (expansion ratio = 2.40). Also, for the massively separated case the tangential wall jet blowing has merged with the wake at the downstream measurement location.

The pressure distributions corresponding to the divergent wall cases do not differ very much from each other (see Fig. 6). The pressure distribution is obtained from pressure taps on the splitter plate and pressure taps on the side-wall of the test section. The pressure distributions are similar between each case due to the displacement effect of the wake (see Fig. 7). The displacement thickness of the wake appears to increase somewhat proportionally to increases in the tunnel divergence. The maximum $-\overline{uv}$ Reynolds shear stress (a measure of the turbulent mixing) increases with distance into the adverse pressure gradient (see Fig. 8).

The $-\overline{uv}$ Reynolds shear stress counteracts the adverse pressure gradient to prevent/postpone flow separation. The greater the Reynolds shear stress gradient the greater the flow's ability to negotiate the adverse pressure gradient without separating. The streamwise

Table 1
Outer edge streamline coordinates used in computations

x (mm)	Symmetric cases					Asymmetric case	
	ER = 1.1 y (mm)	ER = 2.0 y (mm)	ER = 2.25 y (mm)	ER = 2.4 y (mm)	Trailing Edge at $x = 38.1$ mm y (mm)	Upper y (mm)	Lower y (mm)
−723.9	*40.6*	*40.6*	*40.6*	*40.6*	*40.6*	*28.7*	*−32.8*
−469.9	*40.6*	*40.6*	*40.6*	*40.6*	*40.6*	*28.7*	*−32.8*
−215.9	*40.6*	*40.6*	*40.6*	*40.6*	*40.6*	*28.7*	*−32.8*
−88.9	40.6	40.6	40.6	40.6	40.6	28.7	−32.8
−40.6	–	41.7	41.7	41.7	–	–	–
−25.4	–	–	–	–	43.2	29.7	−33.3
0.0	40.9	45.5	43.7	46.5	45.7	34.5	−33.8
38.1	40.1	49.5	51.1	54.9	52.8	44.7	−34.0
76.2	–	–	–	65.8	62.5	–	–
114.3	40.6	61.7	68.3	78.2	72.9	70.4	−34.5
152.4	–	–	77.0	–	–	87.9	−35.6
190.5	40.9	72.9	85.1	100.8	90.2	99.1	−35.8
228.6	–	–	86.4	–	–	–	–
266.7	–	74.9	85.9	101.3	90.2	114.6	−36.6
304.8	–	–	–	99.8	–	116.8	−36.6
342.9	41.1	74.2	84.3	99.1	89.2	115.3	−36.6
419.1	–	74.2	82.6	97.3	87.9	114.0	−36.6
495.3	40.4	75.4	81.3	97.3	86.9	109.5	−35.8
1054.1	*40.4*	*74.2*	*81.3*	*95.5*	*86.9*	*104.1*	*−35.8*

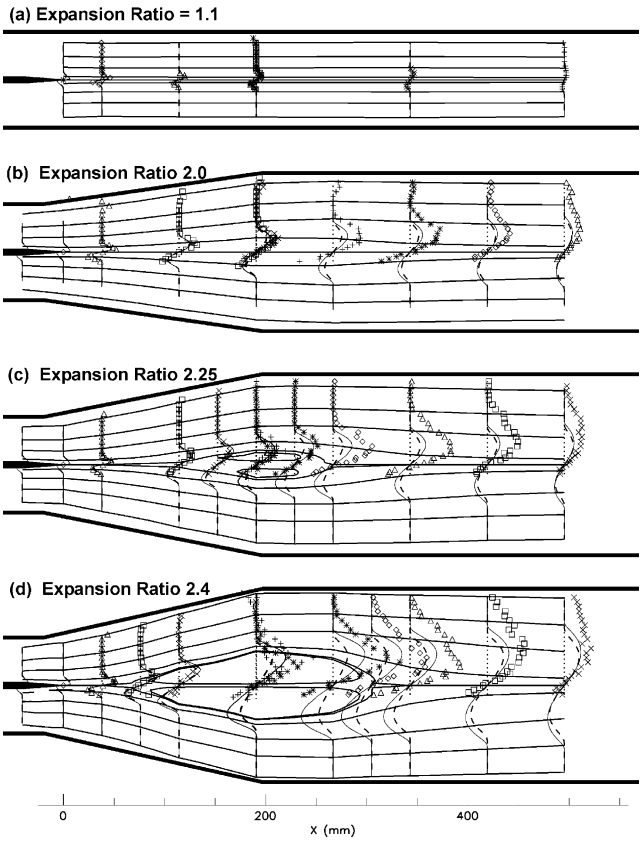

Fig. 5. Measured and computed $-\overline{uv}$ Reynolds shear stress profiles for various tunnel geometries, streamlines overlaid. SST (—), SA (– – –) turbulence models and experiment (symbols).

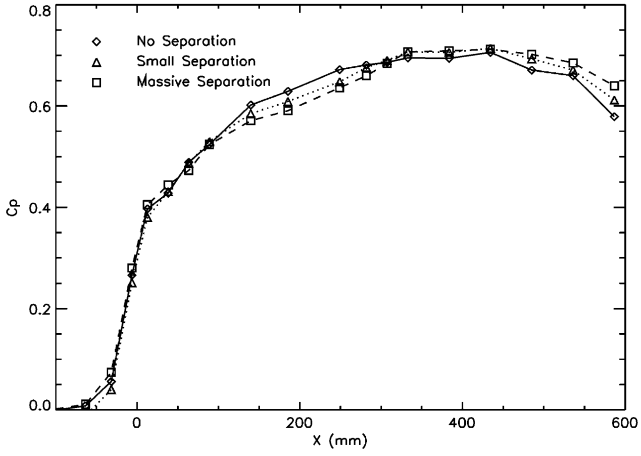

Fig. 6. Pressure distributions.

momentum equation, $U\partial U/\partial x + V\partial U/\partial y = -(1/\rho)\partial p/\partial x - \partial\overline{uv}/\partial y$, shows that where the wake decelerates sufficiently the convection term (left side of equation) becomes negligible. In particular along the centerline and downstream of the splitter plate the measurements show that $V = 0$ (by symmetry) and $U \ll U_\delta$; here the equation reduces to $(1/\rho)\partial p/\partial x = -\partial\overline{uv}/\partial y$. Even

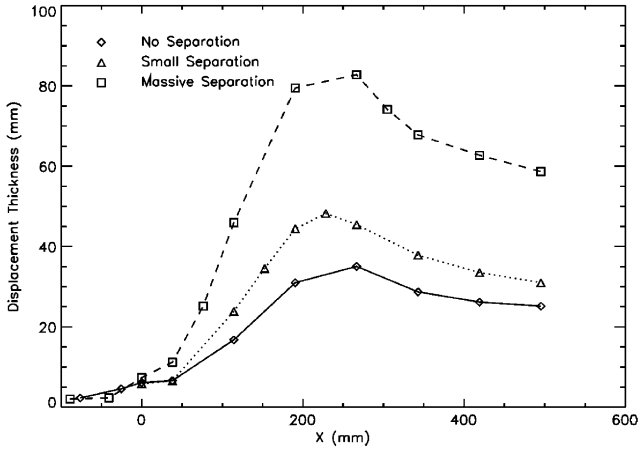

Fig. 7. Displacement thickness distribution.

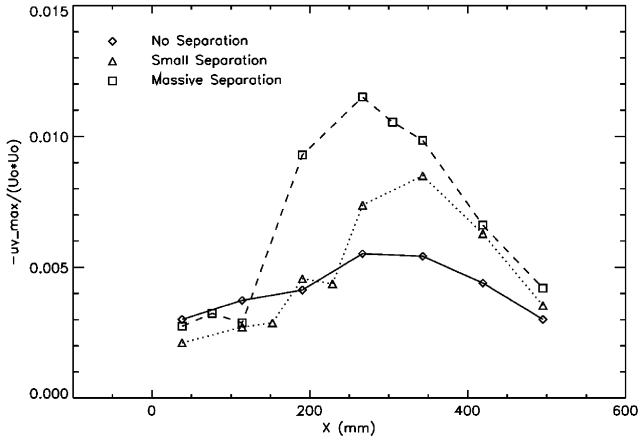

Fig. 8. $-\overline{uv}|_{\max}$ Reynolds stress distribution.

though the Reynolds shear stress is growing with distance along the pressure gradient, it is interesting to note that the Reynolds shear stress gradient along the flow centerline is not significantly altered once the flow is separated (see Fig. 9). In lethargic regions of the flow, the $-\partial\overline{uv}/\partial y$ term is equal to the adverse pressure gradient term and since $-\partial\overline{uv}/\partial y$ is not zero, neither is the pressure gradient (whether the flow is separated or not). Consequently, no "plateau" region (i.e., $\partial p/\partial x = 0$) is seen in the separating flow cases.

Comparison between the experiment and the computations show good qualitative agreement (see Fig. 10). However, for the small separation case neither computation (SST or SA turbulence model) are able to reproduce the flow reversals seen in the experiment. The computed pressure rise (Fig. 10a) is over-predicted by each turbulence model.

The velocity along the centerline ($y = 0$) predicted by each of the models is also higher than in the experiment (Fig. 10b). The stream-wise distribution of local maximum in ($-\overline{uv}$) Reynolds shear stress is also shown

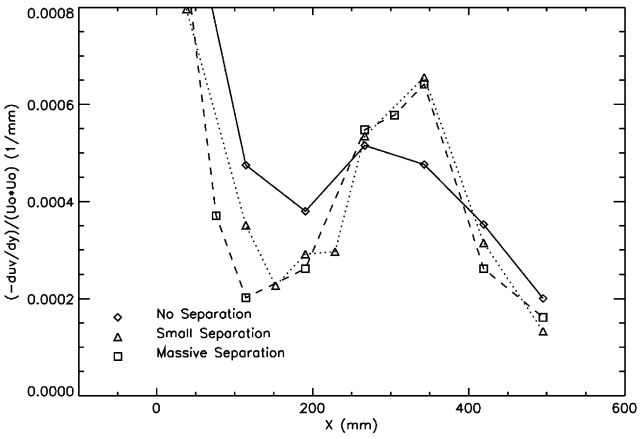

Fig. 9. $-\partial\overline{uv}/\partial y|_{y=0}$ distribution.

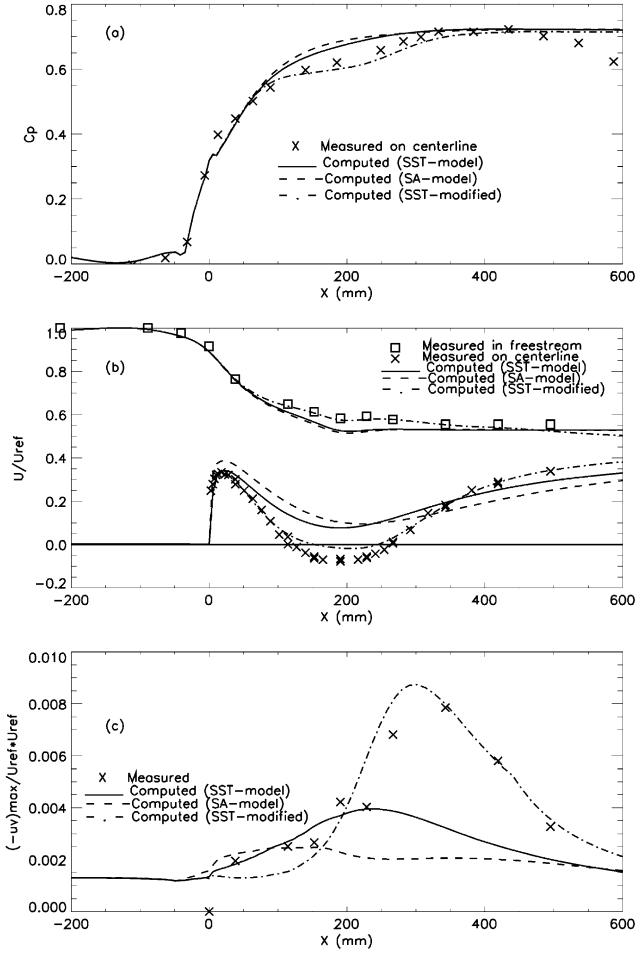

Fig. 10. Pressure, velocity and $-\overline{uv}$ stress evolution for the small separation case (expansion ratio = 2.25).

(Fig. 10c). The Reynolds shear stress ($-\overline{uv}$) computed by each model compares very well in the upstream region of the flow, but downstream neither model is capable of generating the high levels of $-\overline{uv}$ stress seen in the experiment. These high levels of stress seen in the experiment are responsible for the rapid recovery of the centerline velocity in the downstream region.

The failure to predict the displacement effects of the reversed flow region causes the computed pressures to be too high. This overly optimistic prediction of pressure recovery can in turn lead to unrealistically high predictions of lift, as is often the case for computations of high lift multi-element systems of airfoils. Overly optimistic predictions of maximum lift may be in part due to the turbulence model's failure to predict flow reversals in the near-wake as is the case with this experiment.

An additional calculation was performed in which the model was modified to slow the growth of the Reynolds shear stress (eddy viscosity actually), see Fig. 10 (–·– SST modified). An ad hoc modification to INS2D was made in which the eddy viscosity computed by the SST model was multiplied by 0.3 prior to use in the mean flow solver. This modification was applied in a region of the flow between $x = 0$ and 130 mm (smoothly phased in and out). The factor of 0.3 was chosen to obtain a good match to the data. Interestingly, reducing the eddy-viscosity in the upstream region of the flow caused the SST model to produce higher levels of eddy viscosity in the downstream region of the flow where the modification was phased out. This is due to a steeper velocity gradient developed in the wake as a result of a larger velocity deficit. The conclusion is that the biggest deficiency in existing turbulence models is their tendency to over-predict the turbulent eddy-viscosity (Reynolds stress) in the early stages of flow development. Models fail to sufficiently lag the development of the Reynolds stress in response to changes in the mean flow field brought on by adverse pressure gradient.

Additional tests were performed on wakes with curvature and pressure gradient (Fig. 11). The expansion ratio is approximately 2.25, similar to the small separated symmetric case. In this case the plate developed lift with the flow on top of the plate being 1.07 times the nominal reference speed and flow on the bottom of the plate being 0.93 times the nominal reference speed. Here the flow shows less of a velocity deficit in the wake. In the curved case the divergent portion of test section is about 10% longer than in the symmetric case, possibly explaining why there is less of a velocity deficit in the curved case than in the symmetric case. The $-\overline{uv}$ stress shown in Fig. 11 is measured in the laboratory frame of reference (x, y), in this reference frame one sees small differences between the top and bottom half of the wake layer. Rotating to a streamline-oriented frame of reference (not shown) would be more appropriate for drawing conclusions. The computations with the Spalart and Allmaras (1994) turbulence model were run on a 120×162 grid, which covered the full channel (both the top and bottom halves). The inflow condition specified the inlet velocity on top of the splitter plate to be 1.07 U_{ref} and while an inlet velocity of 0.93 U_{ref} was specified

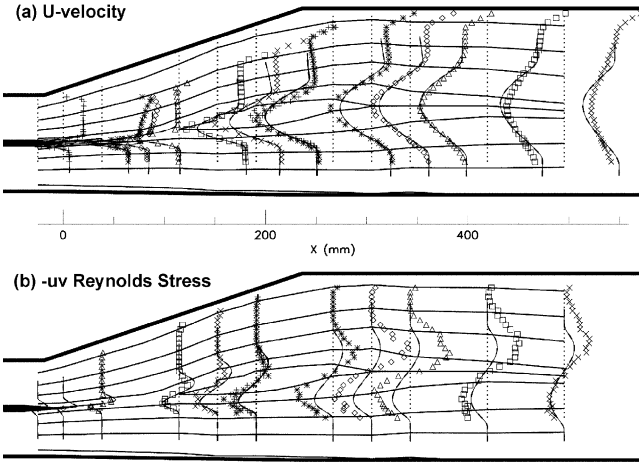

Fig. 11. Wake in an adverse pressure gradient and curvature. Velocity and Reynolds stress measurements (symbols), SA (—) turbulence models.

on the underside of the splitter plate. The computations do not obtain as large a velocity deficit as seen in the experiment in the reversed flow region, also the computations do not generate as large levels of Reynolds shear stress compared to the experiment. This model deficiency is similar to that of the symmetric test cases.

We also studied a case in which the splitter plate was made longer (38 mm longer) so that the trailing edge extended downstream into the diffuser, further into the adverse pressure gradient region of the flow (see Fig. 12). This was done in the interest of simulating the effects of over-hang in a multi-element airfoil system. The expansion ratio was the same as the shorter trailing edge case (ER = 2.25). The separation is similar, but slightly more extensive than the shorter trailing edge case. Larger separation can probably be attributed to the longer length of run that the boundary layer spends in contact with the wall and it's associated skin friction. The models compare a little better with this case, probably due to distance-to-the-surface terms in the models persisting further downstream.

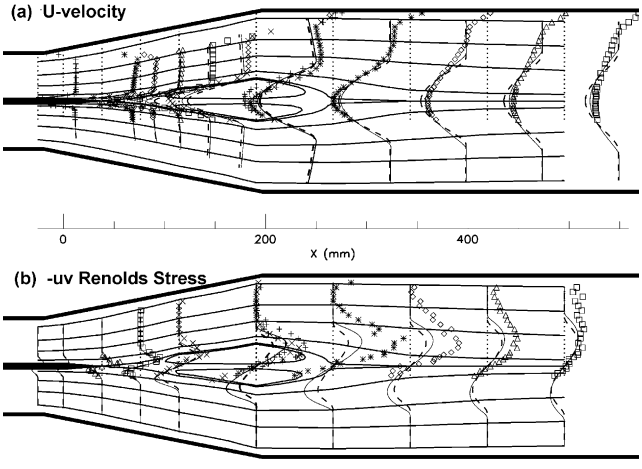

Fig. 12. Extended trailing edge. Velocity and Reynolds stress measurements (symbols), SST (—), SA (– – –) turbulence models.

5. Conclusions

Unique, high quality data were obtained on a two-dimensional wake with flow reversals. Laser-Doppler velocimetry was used to survey velocities and Reynolds stresses in the flow as it encountered various degrees of adverse pressure gradient. Data on flows with varying degrees of reversed flow were obtained. The flows were demonstrated to have good span-wise uniformity and two-dimensionality.

The test cases provide an excellent test bed for CFD validation and turbulence model development. Computations with the SA and the SST (k–ω) turbulence models fail to capture the flow reversals and the associated displacement effects seen in the experiment. Introducing more "lag" into the turbulence model (in an ad hoc way) provided better agreement with the data.

Turbulent Reynolds stresses are seen to increase with increasing wake velocity deficit, however the gradient of $-\overline{uv}$ Reynolds shear stress is not significantly altered by the presence of separation.

References

Adair, D., Horne, C.W., 1988. Characteristics of merging shear layers and turbulent wakes of a multi-element airfoil, NASA TM 100053.

Brune, G.W., Sikavi, D.A., 1983. Experimental investigation of the confluent boundary layer of a multi-element low speed airfoil, AIAA Paper 83-0566.

Chin, V.D., Peters, D.W., Spaid, F.W., McGhee, R.J., 1993. Flowfield measurements about a multi-element airfoil at high Reynolds numbers, AIAA paper 93-3137.

Hoffenberg, R., Sullivan, J.P., and Schneider, S.P., 1995. Wake measurements in a strong adverse pressure gradient, AIAA Paper 95-1912.

Hoffenberg, R., Sullivan, J.P., 1998. Measurement and simulation of a decelerated wake, AIAA Paper 98-0522.

Menter, F.R., 1993. Zonal two equation k-ω turbulence models for aerodynamic flows, AIAA Paper 93-2906.

Pot, P.J., 1979. A wake boundary layer mixing experiment. In: Bradbury, L. (Ed.), Turbulent Shear Flows II. Springer-Verlag, Berlin.

Rogers, S.E., 1993. Progress in high-lift aerodynamic calculations, AIAA Paper 93-0194.

Rogers, S.E., Kwak, D., 1990. An upwind differencing scheme for the time accurate incompressible Navier–Stokes equations. AIAA J. 28 (2), 253–262.

Rogers, S.E., Kwak, D., 1991. An upwind differencing scheme for the steady-state incompressible Navier–Stokes equations. J. Appl. Numer. Math. 8 (1), 43–64.

Roos, F.W., 1997. Experimental studies of wake retardation in a simulated high-lift system flow field, AIAA Paper 97-1813.

Spalart, P., Allmaras, S., 1994. A one-equation turbulence model for aerodynamic flows. La Recherche Aerospatiale 1, 5–21.

Tummers, M.J., Passchier, D.M., Henkes, R.A., 1997. Experimental investigation of an adverse pressure gradient wake and comparison with calculations. Experimental Thermal and Fluid Sci. 14, 24–27.

Xiaofeng, L., Thomas, F.O., Nelson, R.C., 1999. An experimental investigation of wake development in arbitrary pressure gradients. AIAA Paper 99-0677.